

Discovery of New Promising USP14 Inhibitors: Computational Evaluation of the Thumb-palm Pocket.

Niyi Adelakun ^{1*}, Ikponwmosa Obaseki ², Eseiwi Obaseki ³, Ayobami Adeniyi ¹, Oluwaseun Fapohunda ⁴, and Olaposi Omotuyi ^{1 4}.

1. Center for Bio-computing and Drug Development, Adekunle Ajasin University, Akungba-Akoko, Ondo State, Nigeria.
2. Department of Biochemistry, Bell University, Ota, Ogun state, Nigeria.
3. Department of Plant science and Biotechnology, University of Benin, Edo State, Nigeria.
4. Department of Biochemistry, Adekunle Ajasin University, Akungba-Akoko, Ondo State, Nigeria.

Corresponding Author: Niyi Adelakun

email: 130401015@aaua.edu.ng

ABSTRACT

Ubiquitin-specific protease 14 (USP14) is a member of the Deubiquitinating enzymes (DUBs) involved in disrupting the regulation of the ubiquitin-proteasome system, responsible for the degradation of impaired and misfolded proteins which is an essential mechanism in eukaryotic cells. The involvement of USP14 in cancer progression and neurodegenerative disorders has been reported. Thereof USP14 is a prime therapeutic target; hence, designing efficacious inhibitors of USP14 is central in curbing these conditions. Herein, we relied on structural bioinformatics methods incorporating molecular docking, Molecular Mechanics Generalized Born Surface Area (MM-GBSA), Molecular dynamics simulation (MD simulation) and ADME to identify potential allosteric USP14 inhibitors. A library of over 733 compounds from the PubChem repository with >90% match to the IU1 chemical structure was screened in a multi-step framework to attain prospective drug-like inhibitors. Two potential lead compounds (CID 43013232 and CID 112370349) were shown to record better binding affinity compared to IU1, but with subtle difference to IU1-47, a 10-fold potent compound when compared to IU1. The stability of the lead molecules complexed with USP14 was studied via MD simulations. The molecules were found to be stable within the binding site throughout the 50ns simulation time. Moreover, the protein-ligand interactions across the simulation run time suggest Phe331, Tyr476, and Gln197 as crucial residues for USP14 inhibition. Furthermore, *in silico* pharmacological evaluation revealed the lead compounds as pharmacological sound molecules. Overall, the methods deployed in this study revealed two novel candidates that may show selective inhibitory activity against USP14, which could be exploited to produce potent and harmless USP14 inhibitors.

Keywords: USP14; Molecular Docking; Molecular Dynamic simulation; Cancer; Ubiquitin; Drug Discovery

1. Introduction

Protein ubiquitination plays a vital role in the regulation of many cellular processes in eukaryotic cell. They dictate the outcome of proteins by linking different types of polyubiquitin chains [1–4]. Thus far, approximately 100 DUBs have been identified in the human genome and they are involved in regulating several cellular processes and disease states [5]. They are classified into six families, of which the largest is the ubiquitin Specific Protease (USP) family with approximately 60 members [6]. The USPs have a catalytic domain, which includes a highly conserved papain-like fold composed of cysteine, histidine, and aspartate residues [5,6]. The activity of Human USP14 is further stimulated upon proteasome binding via multiple allosteric mechanisms, thus, suppresses global proteasome function. While most studies have been focused on USP14 expression profiles in tumour tissues, the mechanism by which it contributes to tumorigenesis is still being elucidated [7]. Recently, USP14 has been associated with type 2 diabetes mellitus (T2DM) via sustained endoplasmic reticulum stress [8]. Specifically, USP14 overexpression in breast, lungs and pancreatic adenocarcinomas compared to healthy tissues has been confirmed by immunohistochemical investigation. The knockdown of USP14 in cell lines having elevated levels of endogenous USP14 slowed in-vitro proliferation, which resulted in tumour growth inhibition in xenograft studies. In contrast, the reverse was the case in exogenous USP14 expression cell lines [9]. Other studies have shown that catalytically inactive USP14 were found to be essential for sustaining normal functioning of the neuron in ataxia mice [10,11].

Given the role USP14 plays in cancer cell proliferation, research groups have been trying to develop small molecules pronounced in the case of inhibitors against USP14. However, due to the low druggability and conserved nature of these DUBs, previous effort has mainly focused on covalent inhibitors [12,13]. These compounds usually have poor selectivity across the DUB family [13,14]. Finley, king, and co-workers in 2010 reported the first-ever specific inhibitor targeting DUBs, namely IU1, targeting USP14 [14]. It was initially proposed to be an active site-directed protease inhibitor, with its selectivity surprising and puzzling [14]. Recently several findings have revealed other non-covalent inhibitors against DUBs, including XL188 and FT671 [15]. These compounds showed high selectivity for USP7 amongst the DUB family owing to their allosteric regulatory mechanisms. The lack of understanding of the different explanations (covalent for USP 14 versus allosteric for USP 7) for compound selectivity was reconciled by Wang *et al.* [16]. They reported that IU1 exerted its inhibitory activity by binding to the thumb-palm cleft region of the USP14 catalytic domain, which prevented the binding of the C-terminus of ubiquitin to USP14 via obstructing its access to the catalytic center.

Taken together in a broader context, findings indicate that targeting USP14 is of prime importance for the management of neurological disorders and importantly, cancer treatment. IU1 and IU1-47 are the most widely used inhibitors in studying USP14 activity. Availability of the newly determined crystal structure of IU1 complexed with the C-terminal catalytic domain of USP14 (USP14^{CAT}-IU1) aids in accelerating rational compound design against USP14 via allosteric inhibition. Molecular modelling techniques such as Molecular docking, MM-GBSA computation, MD simulation offers a robust solution for predicting intermolecular recognition interactions, hence, identifying potential pharmacological agents [17–20]. Numerous successful applications of molecular modelling pipelines for the identification of promising small-molecules have been recorded [21–23]. To the best of our knowledge, the *in silico* methods utilized so far, have not evaluated the interaction within the thumb-palm region of USP14 by the combination of molecular docking, MM-GBSA calculation, and MD simulations and this is the first study to report on this molecular modelling pipeline.

In this present study, computational methods in a multi-step framework were employed to attain potential drug-like molecules. 733 compounds deposited in the PubChem database with 90% or higher match to the IU1 chemical structure were screened via molecular docking. After careful pose analysis and MM-GBSA calculation, two lead compounds were identified and validated for their stability by MD simulations. Besides, computation of the pharmacological properties of the lead compounds was assessed, displaying satisfactory result. Ultimately, we reveal two novel small molecules that may inhibit USP14 via steric impediment mechanism, which can represent a novel drug in the treatment of cancer.

2. Materials and Methods

2.1 Ligand Library Retrieval

Ligands employed for this study were extracted from PubChem using the IU1 as the target structure to generate compounds with >9.0 tanimoto similarity. Over 733 compounds were retrieved from NCBI PubChem repository [24] in Standard Database Format format (2D). The ligand library retrieved was imported to Maestro and prepared using the Schrodinger suite version 2018-1 [25]. Utilizing Ligprep v4.5 [26], Epik v4.3 [27] with OPLS3 force field [28], for protonation, stereo-isomerization, tautomers generation, and to attain biological conformer. Energy minimization was achieved for all tautomeric states at pH of 7±2.

2.2 Protein Preparation and Grid Generation

Human USP14^{CAT} (1.9 Å) bound to IU1 was retrieved from PDB [29] with the PDB ID 6IHK. Protein Preparation Wizard [30] module in maestro 11.5 was used to prepare the protein complex. Protein structure's missing hydrogen atoms, missing loop, and missing sidechains were fixed while the added hydrogen atoms were optimized at pH 7.0. Optimized structures were minimized using the OPLS3 force field by converging heavy atoms to RMSD of 0.3Å.

The protein binding site was identified by via the receptor grid generation tool in maestro 11.5. Receptor grid defines the region of interaction between the protein and the ligand. The co-crystal ligand was used to identify the binding cavity employing default parameters of van der Waals scaling factor 1.00 and charge cutoff of 0.25 around the binding site residues of the protein structures.

2.3 Docking Studies

Molecular docking studies were performed using Glide v7.8 [25,31] module on maestro 11.5. The ligand library and co-crystal ligand were docked into the binding cavity of the targets using the standard precision algorithm (SP) applying a scaling factor of 0.8 and partial charge cutoff of 0.15, while the ligand was handled as flexible. Extra precision (XP) method was utilized to rerank SP results in order to minimize false-positive [32] Five (5) of the lowest energy poses were selected for post-docking minimization setting the threshold at 0.50 kcal/mol [30]. Lastly, the binding affinity of the receptor-ligand complex was ranked according to Glide score and ligand pose.

To validate our docking protocol, the crystal ligand (IU1) was extracted from the complex, prepared and docked back to the thumb-palm cleft section distant from the catalytic site of USP14 using the same protocol. The resulted pose was calculated in terms of RMSD. It is evident from the RMSD value of 1.7 Å that the redocking conformation of IU1 is in good agreement with the corresponding bound orientation (Supplementary **Figure S1**). According to literature, to validate a docking protocol, the RMSD value between the redocked and native ligand should be less than 2 Å [33].

2.4 Binding Free Energy Calculations Using MM-GBSA

The Prime/MM-GBSA module [34] of the Schrodinger suite was applied to calculate the binding free energies of the docked complexes. Outputs of docked complexes from XP method were used to calculate the binding free energy as previously described [34,35]

2.4 Molecular Dynamic Simulations

All MD simulation was run on Desmond program [36,37]. Briefly, docked complexes were solvated in an orthorhombic box of TIP3 water model, 0.15 M NaCl was incorporated into each system to neutralize the charges and also to mimic physiological conditions. The smooth particle mesh Ewald (PME) estimation [38] was employed for long-range electrostatics, while MSHAKE algorithm [39] was utilized for nonbonded interactions at 9 Å cut-off. The systems were relaxed applying the default Desmond protocol [36]. During the first two steps, a minimization with restrains on solute heavy atoms, followed by minimization without

restraints was deployed, using the Broyden-Fletcher-Goldfarb Shanno (LBFGS) algorithms [41], with a convergence threshold of 1.0 kcal/mol/Å. In the next two steps, equilibration was performed through NVT and NPT ensembles with restraint on the solute heavy atoms at 10 K and time interval of 12ps of Berendsen dynamics. The final two steps of equilibration were by NPT ensemble with and without restraints on the solute heavy atoms for 12ps and 24ps time gap at temperature 300 K, respectively, using Berendsen dynamics [42]. Consequently, 50ns production run of the relaxed system was carried out with NPT ensemble; the temperature was maintained at 300 K by Nose-Hoover thermostat [43] while the pressure was conserved at 1 atm via Martyna-Tuckerman-Klein barostat [44]. The trajectories were computed using a multiple time step RESPA integrator, to solve the short-range bonded and long-range non-bonded interactions at 2.0fs and 6.0fs, respectively. Simulation results analysis were performed using the Desmond SID in maestro [37]. The raw data were extracted while the graphs were plotted using GraphPad Prism (Version 8) [46].

2.5 ADME Evaluation

The absorption, distribution, metabolism, and excretion of the lead molecules were predicted using the Qikprop module in maestro 11.5. QikProp predicts physically significant descriptors and pharmaceutically features of organic molecules. It uses descriptors that are gotten from the molecular structure and calculated molecular properties [40].

3. Results and Discussion

3.1 Molecular docking, MM-GBSA binding energy and Interaction profiling of USP14^{CAT}-Ligand complexes

The USP14^{CAT}-IU1 crystal structure [16] has provided a high resolution starting pose to help expedite the search of small molecules that may inhibit USP14 by blocking the S1 site, thereby resulting to the steric impediment of the C-terminus of ubiquitin to its active site. Chemical structures with similar geometry would provide comparable effects [45] Thus, 733 compounds from the PubChem database with 9.0 or higher tanimoto coefficient match to the IU1 chemical structure was employed to study their binding affinity and binding orientation against USP14 by molecular docking. The logic for the method (selected compounds for screening) used is to discover small molecules that are selective to USP14 and would fit into its IU1 binding site (thumb-palm cleft) owing to the snug nature of this cleft [47], which might doubtfully accommodate larger compounds. The docking protocol was streamlined through SP and XP-docking methods to attain potential lead compounds. From the 733 compounds docked and scored using the SP mode, 30% (219) of the top-ranked compounds obtained were redocked and rescored with the XP Gscore to minimize false positives [45]. The minimum cut-off for active compounds was set at Gscore \leq -7. 200 kcal/mol. Ten docked complexes that passed the threshold were post-scored with Prime/MM-GBSA. Post-scoring molecules with Prime/MM-GBSA have been shown to have a better correlation to their experimental binding affinity when compared to XP Gscore [32,48,49]. Based on MM-GBSA binding energy (ΔG_{bind}), together with molecules π - π or π -cation interactions with conserved amino acid residues (His426, Tyr436, and Tyr476) of USP14, CID 43013232 and CID 112370349 emerged as

promising compounds (**Figure 1**). Hence, were selected together with the known USP14 Inhibitors (IU1 and IU1-47) for their interaction profile analysis.

From the XP Gscore, CID 43013232 and CID 112370349 recorded a Gscore of -8.047 kcal/mol and -7.428 kcal/mol, respectively when compared to the co-crystal ligand (IU1) which recorded -6.439 kcal/mol. Here, only CID 43013232 scored better than IU1-47 (-7.496 kcal/mol), although the Gscore between CID 112370349 was subtle (**Figure 2**). However, because XP Gscore is an empirical score, we wanted to confirm this report by MM-GBSA binding energy. Following MM-GBSA computation of the docked poses, CID 43013232, CID 112370349, IU1, and IU1-47, binding energies (ΔG_{bind}) were estimated as -62.78, -58.78, -51.10, -65.63 (kcal/mol) respectively (**Figure 2**). The values recorded for binding energy disclosed that the two lead compounds and IU1-47 docked favorably to the thumb-palm cleft of USP14 when compared to IU1. Interestingly, the binding energy of IU1-47, but not IU1, an improved analogue of IU1, was better than CID 112370349; nonetheless, it showed comparable outcome with CID 43013232 which is consistent with the XP Gscore. Notably, IU1-47 showed superiority when compared to IU1; this is in good agreement with King, Finley and colleagues, and Wang, Jiang *et al.* experimental results, which revealed 10-fold potency over IU1 [16,50].

The thumb-palm cleft of USP14 is composed of hydrophobic, conserved residues. Phe331, Tyr333, His426, Tyr436, and Tyr476 residues are responsible for the crucial recognition of USP14 inhibitors, thereby inhibiting the enzyme activities via obstructing the access of the C-terminus of ubiquitin to the active site residues. The blocking loop 1 (330-342) and blocking loop 2 (429-433), are associated with auto-inhibition of USP14 in its free state, and stabilization of ubiquitin to the catalytic center when associated with proteasome [7,16,51]. The known inhibitors (IU1 and IU1-47) positioned their aromatic ring containing the electron-withdrawing halogen to make hydrophobic interactions with Phe331, Tyr 436, and Tyr 476, although, Leu196 was in contact with IU1-47, but not with IU1 (**Table 1**). Understandably, the Cl- on the phenyl ring of IU1-47 is larger than that of the F- group on IU1, aiding IU1-47 robust fitting into the same pocket, enjoying stronger hydrophobic interactions which are similar to Wang and colleagues report [16]. Without a doubt, IU1 and IU1-47 both made π -cation interactions with key amino acid residues His426 (**neutral His**) and Tyr 476. However, IU1 made two H-bond interactions with Tyr436. In contrast, the NH⁺ on pyrrolidine ring of IU1-47 and the O on the alkyl linker revealed H-bond contact with Gln197 on the switching loop (SWL); additionally, IU1-47 provided stabilization via H-bonding with Ser431. Indeed, the hydrogen bonds, the Cl- on the phenyl ring together with the large pyrrolidine ring, were available for van der Waals interaction within the hydrophobic pocket of the thumb-palm cleft, which might also explain the 10-fold potency over IU1.

The 3D superimposition revealed that the lead compounds occupy similar binding orientation as IU1 and IU1-47 with reasonable alignment in the USP14 binding pocket. Understandably, they share a notable number of structural resemblance (9.0 tanimoto coefficient) with the crystal ligand. However, the benzene ring is further spaced away from the pyrrole ring, while a hydroxymethyl group is attached to the pyrrolidine ring of CID 112370349. In contrast, the one position of the piperazine ring of CID 43013232 has a 1-(but-1-en-2-yl)pyrrolidine functional group. These different functional groups have a notable impact upon the observed binding modes of each lead compound in the pocket. For instance, the hydroxymethyl group of CID 112370349 was oriented to form H-bond with Ser432 located on BL2. Interestingly, an *in vitro* and cell-based assay conducted by Xu et al. revealed that phosphorylation at Ser432 by AKT triggers inactive USP14, as well as increases the activity of proteasome-bound USP14 [52]. Hence, this interaction is crucial for USP14 inhibition. Moreover, USP14^{CAT}-CID 112370349 complex was

also sustained by H-bond contact with Gln197, π - π interactions with Hie426 and Lys342, and hydrophobic interaction with similar residues with IU1-47(see **Table 1**, **Figure 1d**). CID 43013232 maintained stability by π - π stacking with Hie426 and Tyr476. Notably, CID 43013232 enjoyed more hydrophobic interactions (Phe186, Leu196, Phe331, Tyr 436, and Tyr 476) when compared to other candidates, which might be the significant contributor to its superior docking score and binding energy (**Figure 1c**). Plausibly, its multiple aromatic rings with suitable alkyl linkers are available for van der Waals interactions with the hydrophobic-rich amino acids within the binding pocket, unlike the compact pyrrolidine ring on IU1.

3.2 Molecular Dynamic Simulations of USP14^{CAT}-Ligand Complexes

The apo state and selected docked complexes were utilized as the starting coordinate to perform MD simulations intending to verify the conformational stability of the ligands within the binding pocket of USP14. Each molecule's RMSD, RMSF, and Ligand binding site residue were evaluated. The USP14^{CAT}-ligand RMSD over 50ns for all the complexes are shown in **Figure 3**. The RMSD C α values for apo state were within 1.20 Å to 2.8 Å, while the average RMSD asymmetric carbon was 2.02 Å. It was observed that the RMSD C α atom of USP14^{CAT} in all the selected complexes was relatively steady in all of the simulations ranging from 1.30 Å to 3.3 Å with average values of 2.336, 2.092, 2.126, and 2.178 Å for IU1, IU1-47, CID 43013232, and CID 112370349 respectively. Next, each ligand's RMSD within the enzyme was calculated to determine their stability (**Figure 3**). Notably, IU1, IU1-47, and CID 112370349 oscillated between 0.6 Å to 2.2 Å with an average value of about 1.3 Å. Conversely, CID 43013232 displayed slight fluctuation, averaging around 2.3 Å, which might be as a result of the number of rotatable bonds and the 1-(but-1-en-2-yl)pyrrolidine functional group which protrudes outward of the compact pocket.

RMSF was used to monitor local changes along the USP14^{CAT} amino acid residues for the 50ns simulation run time. It was observed that the alpha helices and beta strands of the apo structure and docked complexes oscillated within 0.8 Å to 1.5 Å. As shown in (**Figure 4**), loop regions of all the systems experienced large fluctuations up to 5.8 Å. Notably, there were no significant instabilities in the loop regions while comparing within systems. Interestingly, the BL2, BL1, and SWL experienced fluctuation averaging from 2.8, 4.3, and 2.3, respectively. Logically, the high fluctuations of the loops recorded were due to their inherent flexible nature; clearly, the reduced changes observed might be associated with the ligand interactions observed within these regions. From the above results, CID 43013232 and CID 112370349 were found to be extremely stable in the binding pocket with minimal structural rearrangements and lesser conformational changes to the overall enzyme structure, rendering them suitable inhibitors.

Furthermore, we took into account the time dependencies of USP14^{CAT}-Ligands contacts by comparing their interactions with the amino acid residues across the entire simulation. Unlike the binding orientation obtainable by molecular docking, MD simulation aids in evaluating all the binding modes by averaging all protein-ligand interactions gotten from individual frames of the simulations and determines the most favorable interactions. Intriguingly, all the complexes (IU1, IU1-47, CID 43013232, and CID 112370349) subjected to MD simulation share quite a few conserved interactions that were sustained all through the simulation (**Figure 5**). These conserved interactions are hydrophobic contacts with amino acid residues Phe331, Tyr476, Tyr 436, Hie426, and H-bond contacts with Gln197. Notably, involvement with phe331, Tyr467, and Gln197 was observed from 50% to 70% of the simulation time. Conversely, contacts maintained with Hie426 and Tyr436 were minimal (below 20%) and showed no significant difference when compared across all systems. In contrast, only IU1 made Ionic contact, H-bond, and H-bonding facilitated

by a water bridge at over 70% with Asp199, which is resident at the SWL. Besides, IU1-47 (H-bond) and CID 43013232 (H-bond mediate by water) were capable of maintaining interaction with Ser431 for up to 70% and 40%, respectively. CID 43013232 was the only compound that sustained interaction with BL1, interacting with Lys342 via H-bond facilitated by water molecules and hydrophobic contact for about 60% over the 50ns simulation. Ultimately CID 112370349 alone was capable of communication with Ser432 (residue liable to activation by AKT) via both H-bond and water-mediated H-bond. The enhanced docking score and binding energy recorded for CID 43013232 and IU1-47 may be explained by the Hydrophobic interaction with Phe331 at about 100% and 80%, respectively. Interestingly, Phe331 position is equivalent to the Phe409 residue in USP7, a homolog of USP14 [7,51], which is a key interacting residue for potent allosteric inhibitors of USP7 [7,12,53]. Finally, the weak docking score and binding energy recorded for IU1 were in line with the observation that none of the interactions with crucial residues accounted for more than 50% of the entire simulation.

The attained data from MD simulations demonstrate that Phe331, Tyr476, and Gln197 are possible essential amino acid residues for USP14 allosteric inhibition. It also corroborates with the hypothesis that IU series binds to the thumb-palm region of USP14 and does not trigger an overall conformational change. Prominently, CID 43013232, and CID 112370349 were stable in the binding site and may efficiently sterically impede the access of the C-terminus of ubiquitin to the USP14 catalytic center. However, further studies will be required to definitely prove the activity CID 43013232 and CID 112370349 as a novel USP14 inhibitors.

3.3 Drug-Likeness and ADME Evaluation

The pharmacological properties of the lead compounds were evaluated to predict their physiochemical and biological features. To estimate oral availability, Christopher Lipinski proposed rules of five (Ro5: molecular weight (MW <500), number of hydrogen bond donor (HBD <5), number of hydrogen bond acceptor (HBA <10), and predicted octanol/ water partition coefficient ($\log P < 5$) was employed [54]. As displayed in **Table 2** the lead compounds didn't violate any of the rules, which supports them as potentially druggable molecules. Next, the ADME features of the lead compounds were determined to capture their pharmacological competence [55]. The results indicate that 77% of CID 43013232 and 91.8% of CID 112370349 will be well absorbed. Moreover, they both have low binding affinity to serum, therefore increasing their availability in blood circulation for efficient diffusion into cell membranes and dynamic binding to their target. **Table 2** shows that the compounds are within the accepted value for Blood-brain barrier and Madin-Darby canine kidney parameter, thus showing the ability to cross the blood-brain barrier through passive transport without upsetting CNS activity [56]. The accessibility level of the compounds towards their target after entering into the bloodstream was determined by predicting their likely number of metabolic reactions. The results showed that they are all metabolically inactive. According to the results displayed in **Table 2**, both the lead and reference compounds fell between the accepted ranges for all the calculated pharmacological parameters.

4. Conclusions

USP14 is an essential clinical target, which has been implicated in oncology, neurodegenerative diseases, and, most recently T2DM. IU1 and IU1-47 are the most studied compounds used to demonstrate USP14 inhibition; today, new insight into the binding mode of IU series has been provided by x-ray structures. In this study, computational approaches were employed to discover novel compounds having analogous scaffold as IU series. Molecular docking results showed that CID 43013232 and CID 112370349 bind to the thumb-palm cleft of USP14, interacting with essential amino acid residues necessary for inhibition with favorable binding affinity. Our atomistic simulations data validates their stability within the binding pocket and also suggests Phe331, Tyr476 and Gln197 as crucial residues for USP14 inhibition. Moreover, the compounds were subjected to *in silico* pharmacological evaluation and were found to be suitable. Thus, our study identified CID 43013232 and CID 112370349 as potential drug contender against USP14. Nonetheless, to further validate our findings *in vivo* and or *in vitro* experiments could be examined to establish their potential to inhibit USP14.

References

1. Hershko, A.; Ciechanover, A.; Varshavsky, A. Basic Medical Research Award. The ubiquitin system. *Nat. Med.* **2000**, *6*, 1073–1081, doi:10.1038/80384.
2. Glickman, M.H.; Ciechanover, A. The ubiquitin-proteasome proteolytic pathway: Destruction for the sake of construction. *Physiol. Rev.* **2002**, *82*, 373–428, doi:10.1152/physrev.00027.2001.
3. Goldberg, A.L. Functions of the proteasome: From protein degradation and immune surveillance to cancer therapy. *Biochem. Soc. Trans.* **2007**, *35*, 12–17, doi:10.1042/BST0350012.
4. Matyskiela, M.E.; Martin, A. Design principles of a universal protein degradation machine. *J. Mol. Biol.* **2013**, *425*, 199–213, doi:10.1016/j.jmb.2012.11.001.
5. Fraile, J.M.; Quesada, V.; Rodríguez, D.; Freije, J.M.P.; López-Otín, C. Deubiquitinases in cancer: New functions and therapeutic options. *Oncogene* **2012**, *31*, 2373–2388, doi:10.1038/onc.2011.443.
6. Nijman, S.M.B.; Luna-Vargas, M.P.A.; Velds, A.; Brummelkamp, T.R.; Dirac, A.M.G.; Sixma, T.K.; Bernards, R. A genomic and functional inventory of deubiquitinating enzymes. *Cell* **2005**, *123*, 773–786, doi:10.1016/j.cell.2005.11.007.
7. Wertz, I.E.; Murray, J.M. Structurally-defined deubiquitinase inhibitors provide opportunities to investigate disease mechanisms. *Drug Discov. Today Technol.* **2019**, *31*, 109–123, doi:10.1016/j.ddtec.2019.02.003.
8. Liu, B.; Zhang, Z.; Hu, Y.; Lu, Y.; Li, D.; Liu, J.; Liao, S.; Hu, M.; Wang, Y.; Zhang, D.; et al. Sustained ER stress promotes hyperglycemia by increasing glucagon action through the deubiquitinating enzyme USP14. *Proc. Natl. Acad. Sci. U. S. A.* **2019**, *116*, 21732–21738, doi:10.1073/pnas.1907288116.
9. Zhu, Y.; Zhang, C.; Gu, C.; Li, Q.; Wu, N. Function of Deubiquitinating Enzyme USP14 as Oncogene in Different Types of Cancer. *Cell. Physiol. Biochem.* **2016**, *38*, 993–1002, doi:10.1159/000443051.

10. Bhattacharyya, B.J.; Wilson, S.M.; Jung, H.; Miller, R.J. Altered neurotransmitter release machinery in mice deficient for the deubiquitinating enzyme Usp14. *Am. J. Physiol. , Cell Physiol.* **2012**, *302*, C698-708, doi:10.1152/ajpcell.00326.2010.
11. Walters, B.J.; Hallengren, J.J.; Theile, C.S.; Ploegh, H.L.; Wilson, S.M.; Dobrunz, L.E. A catalytic independent function of the deubiquitinating enzyme USP14 regulates hippocampal synaptic short-term plasticity and vesicle number. *J. Physiol. (Lond)* **2014**, *592*, 571–586, doi:10.1113/jphysiol.2013.266015.
12. Turnbull, A.P.; Ioannidis, S.; Krajewski, W.W.; Pinto-Fernandez, A.; Heride, C.; Martin, A.C.L.; Tonkin, L.M.; Townsend, E.C.; Buker, S.M.; Lancia, D.R.; et al. Molecular basis of USP7 inhibition by selective small-molecule inhibitors. *Nature* **2017**, *550*, 481–486, doi:10.1038/nature24451.
13. Wang, X.; D'Arcy, P.; Caulfield, T.R.; Paulus, A.; Chitta, K.; Mohanty, C.; Gullbo, J.; Chanan-Khan, A.; Linder, S. Synthesis and evaluation of derivatives of the proteasome deubiquitinase inhibitor b-AP15. *Chem. Biol. Drug Des.* **2015**, *86*, 1036–1048, doi:10.1111/cbdd.12571.
14. Lee, B.-H.; Lee, M.J.; Park, S.; Oh, D.-C.; Elsasser, S.; Chen, P.-C.; Gartner, C.; Dimova, N.; Hanna, J.; Gygi, S.P.; et al. Enhancement of proteasome activity by a small-molecule inhibitor of USP14. *Nature* **2010**, *467*, 179–184, doi:10.1038/nature09299.
15. Lamberto, I.; Liu, X.; Seo, H.-S.; Schauer, N.J.; Jacob, R.E.; Hu, W.; Das, D.; Mikhailova, T.; Weisberg, E.L.; Engen, J.R.; et al. Structure-Guided Development of a Potent and Selective Non-covalent Active-Site Inhibitor of USP7. *Cell Chem. Biol.* **2017**, *24*, 1490-1500.e11, doi:10.1016/j.chembiol.2017.09.003.
16. Wang, Y.; Jiang, Y.; Ding, S.; Li, J.; Song, N.; Ren, Y.; Hong, D.; Wu, C.; Li, B.; Wang, F.; et al. Small molecule inhibitors reveal allosteric regulation of USP14 via steric blockade. *Cell Res.* **2018**, *28*, 1186–1194, doi:10.1038/s41422-018-0091-x.
17. Kitchen, D.B.; Decornez, H.; Furr, J.R.; Bajorath, J. Docking and scoring in virtual screening for drug discovery: Methods and applications. *Nat. Rev. Drug Discov.* **2004**, *3*, 935–949, doi:10.1038/nrd1549.
18. Omotuyi, O.I.; Nash, O.; Safronetz, D.; Ojo, A.A.; Ogunwa, T.H.; Adelakun, N.S. T-705-modified ssRNA in complex with Lassa virus nucleoprotein exhibits nucleotide splaying and increased water influx into the RNA-binding pocket. *Chem. Biol. Drug Des.* **2019**, *93*, 544–555, doi:10.1111/cbdd.13451.
19. Kwofie, S.K.; Dankwa, B.; Enniful, K.S.; Adobor, C.; Broni, E.; Ntiamoah, A.; Wilson, M.D. Molecular Docking and Dynamics Simulation Studies Predict Munc18b as a Target of Mycolactone: A Plausible Mechanism for Granule Exocytosis Impairment in Buruli Ulcer Pathogenesis. *Toxins (Basel)* **2019**, *11*, doi:10.3390/toxins11030181.
20. Wade, R.C.; Salo-Ahen, O.M.H. Molecular Modeling in Drug Design. *Molecules* **2019**, *24*, doi:10.3390/molecules24020321.
21. Ghamari, N.; Zarei, O.; Reiner, D.; Dastmalchi, S.; Stark, H.; Hamzeh-Mivehroud, M. Histamine H3 receptor ligands by hybrid virtual screening, docking, molecular dynamics simulations, and investigation of their biological effects. *Chem. Biol. Drug Des.* **2019**, *93*, 832–843, doi:10.1111/cbdd.13471.
22. Ma, Y.; Wang, S.-Q.; Xu, W.-R.; Wang, R.-L.; Chou, K.-C. Design novel dual agonists for treating type-2 diabetes by targeting peroxisome proliferator-activated receptors with core hopping approach. *PLoS ONE* **2012**, *7*, e38546, doi:10.1371/journal.pone.0038546.

23. Selvakumar, J.N.; Chandrasekaran, S.D.; Doss, G.P.C.; Kumar, T.D. Inhibition of the ATPase Domain of Human Topoisomerase IIa on HepG2 Cells by 1, 2-benzenedicarboxylic Acid, Mono (2-ethylhexyl) Ester: Molecular Docking and Dynamics Simulations. *Curr. Cancer Drug Targets* **2019**, *19*, 495–503, doi:10.2174/1568009619666181127122230.
24. Kim, S.; Thiessen, P.A.; Bolton, E.E.; Chen, J.; Fu, G.; Gindulyte, A.; Han, L.; He, J.; He, S.; Shoemaker, B.A.; et al. PubChem Substance and Compound databases. *Nucleic Acids Res.* **2016**, *44*, D1202-13, doi:10.1093/nar/gkv951.
25. Maestro, Schrödinger, LLC, New York, NY, **2018**.
26. LigPrep, Schrödinger, LLC, New York, NY, **2018**.
27. Greenwood, J.R.; Calkins, D.; Sullivan, A.P.; Shelley, J.C. Towards the comprehensive, rapid, and accurate prediction of the favorable tautomeric states of drug-like molecules in aqueous solution. *J. Comput. Aided Mol. Des.* **2010**, *24*, 591–604, doi:10.1007/s10822-010-9349-1.
28. Harder, E.; Damm, W.; Maple, J.; Wu, C.; Reboul, M.; Xiang, J.Y.; Wang, L.; Lupyan, D.; Dahlgren, M.K.; Knight, J.L.; et al. OPLS3: A Force Field Providing Broad Coverage of Drug-like Small Molecules and Proteins. *J. Chem. Theory Comput.* **2016**, *12*, 281–296, doi:10.1021/acs.jctc.5b00864.
29. Berman, H.M.; Westbrook, J.; Feng, Z.; Gilliland, G.; Bhat, T.N.; Weissig, H.; Shindyalov, I.N.; Bourne, P.E. The Protein Data Bank. *Nucleic Acids Res.* **2000**, *28*, 235–242, doi:10.1093/nar/28.1.235.
30. Sastry, G.M.; Adzhigirey, M.; Day, T.; Annabhimoju, R.; Sherman, W. Protein and ligand preparation: Parameters, protocols, and influence on virtual screening enrichments. *J. Comput. Aided Mol. Des.* **2013**, *27*, 221–234, doi:10.1007/s10822-013-9644-8.
31. Friesner, R.A.; Banks, J.L.; Murphy, R.B.; Halgren, T.A.; Klicic, J.J.; Mainz, D.T.; Repasky, M.P.; Knoll, E.H.; Shelley, M.; Perry, J.K.; et al. Glide: A new approach for rapid, accurate docking and scoring. 1. Method and assessment of docking accuracy. *J. Med. Chem.* **2004**, *47*, 1739–1749, doi:10.1021/jm0306430.
32. Tripathi, S.K.; Muttineni, R.; Singh, S.K. Extra precision docking, free energy calculation and molecular dynamics simulation studies of CDK2 inhibitors. *J. Theor. Biol.* **2013**, *334*, 87–100, doi:10.1016/j.jtbi.2013.05.014.
33. Kamchonwongpaisan, S.; Quarrell, R.; Charoensetakul, N.; Ponsinet, R.; Vilaivan, T.; Vanichtanankul, J.; Tarnchompoo, B.; Sirawaraporn, W.; Lowe, G.; Yuthavong, Y. Inhibitors of multiple mutants of Plasmodium falciparum dihydrofolate reductase and their antimalarial activities. *J. Med. Chem.* **2004**, *47*, 673–680, doi:10.1021/jm030165t.
34. Prime, Schrödinger, LLC, New York, NY, 2019. Prime, Schrödinger, LLC, New York, NY, **2018**.
35. Genheden, S.; Ryde, U. The MM/PBSA and MM/GBSA methods to estimate ligand-binding affinities. *Expert Opin. Drug Discov.* **2015**, *10*, 449–461, doi:10.1517/17460441.2015.1032936.
36. Bowers, K.J.; Chow, D.E.; Xu, H.; Dror, R.O.; Eastwood, M.P.; Gregersen, B.A.; Klepeis, J.L.; Kolossvary, I.; Moraes, M.A.; Sacerdoti, F.D.; et al. Scalable Algorithms for Molecular Dynamics Simulations on Commodity Clusters. In *ACM/IEEE SC 2006 Conference (SC'06)*. SC 2006 Proceedings Supercomputing 2006, Tampa, FL; IEEE, 2006; p 43.
37. Maestro-Desmond Interoperability Tools, Schrödinger, New York, NY, **2018**.
38. Darden, T.; York, D.; Pedersen, L. Particle mesh Ewald: An $N \cdot \log(N)$ method for Ewald sums in large systems. *The Journal of Chemical Physics* **1993**, *98*, 10089–10092, doi:10.1063/1.464397.
39. Lambrakos, S.G.; Boris, J.P.; Oran, E.S.; Chandrasekhar, I.; Nagumo, M. A modified shake algorithm for maintaining rigid bonds in molecular dynamics simulations of large molecules. *Journal of Computational Physics* **1989**, *85*, 473–486, doi:10.1016/0021-9991(89)90160-5.

40. QikProp, Schrödinger LLC, New York, NY, **2018**.
41. Head, J.D.; Zerner, M.C. A Broyden—Fletcher—Goldfarb—Shanno optimization procedure for molecular geometries. *Chemical Physics Letters* **1985**, *122*, 264–270, doi:10.1016/0009-2614(85)80574-1.
42. Berendsen, H.J.C.; Postma, J.P.M.; van Gunsteren, W.F.; DiNola, A.; Haak, J.R. Molecular dynamics with coupling to an external bath. *The Journal of Chemical Physics* **1984**, *81*, 3684–3690, doi:10.1063/1.448118.
43. Nosé, S. A unified formulation of the constant temperature molecular dynamics methods. *The Journal of Chemical Physics* **1984**, *81*, 511–519, doi:10.1063/1.447334.
44. Martyna, G.J.; Tobias, D.J.; Klein, M.L. Constant pressure molecular dynamics algorithms. *The Journal of Chemical Physics* **1994**, *101*, 4177–4189, doi:10.1063/1.467468.
45. Friesner, R.A.; Murphy, R.B.; Repasky, M.P.; Frye, L.L.; Greenwood, J.R.; Halgren, T.A.; Sanschagrin, P.C.; Mainz, D.T. Extra precision glide: Docking and scoring incorporating a model of hydrophobic enclosure for protein-ligand complexes. *J. Med. Chem.* **2006**, *49*, 6177–6196, doi:10.1021/jm051256o.
46. GraphPad Prism. GraphPad Software, La Jolla California USA, www.graphpad.com” **2019**.
47. Kategaya, L.; Di Lello, P.; Rougé, L.; Pastor, R.; Clark, K.R.; Drummond, J.; Kleinheinz, T.; Lin, E.; Upton, J.-P.; Prakash, S.; et al. USP7 small-molecule inhibitors interfere with ubiquitin binding. *Nature* **2017**, *550*, 534–538, doi:10.1038/nature24006.
48. Greenidge, P.A.; Kramer, C.; Mozziconacci, J.-C.; Wolf, R.M. MM/GBSA binding energy prediction on the PDBbind data set: Successes, failures, and directions for further improvement. *J. Chem. Inf. Model.* **2013**, *53*, 201–209, doi:10.1021/ci300425v.
49. Lyne, P.D.; Lamb, M.L.; Saeh, J.C. Accurate prediction of the relative potencies of members of a series of kinase inhibitors using molecular docking and MM-GBSA scoring. *J. Med. Chem.* **2006**, *49*, 4805–4808, doi:10.1021/jm060522a.
50. Boselli, M.; Lee, B.-H.; Robert, J.; Prado, M.A.; Min, S.-W.; Cheng, C.; Silva, M.C.; Seong, C.; Elsasser, S.; Hatle, K.M.; et al. An inhibitor of the proteasomal deubiquitinating enzyme USP14 induces tau elimination in cultured neurons. *J. Biol. Chem.* **2017**, *292*, 19209–19225, doi:10.1074/jbc.M117.815126.
51. Hu, M.; Li, P.; Song, L.; Jeffrey, P.D.; Chenova, T.A.; Wilkinson, K.D.; Cohen, R.E.; Shi, Y. Structure and mechanisms of the proteasome-associated deubiquitinating enzyme USP14. *EMBO J.* **2005**, *24*, 3747–3756, doi:10.1038/sj.emboj.7600832.
52. Xu, D.; Shan, B.; Lee, B.-H.; Zhu, K.; Zhang, T.; Sun, H.; Liu, M.; Shi, L.; Liang, W.; Qian, L.; et al. Phosphorylation and activation of ubiquitin-specific protease-14 by Akt regulates the ubiquitin-proteasome system. *Elife* **2015**, *4*, e10510, doi:10.7554/eLife.10510.
53. Gavory, G.; O'Dowd, C.R.; Helm, M.D.; Flasz, J.; Arkoudis, E.; Dossang, A.; Hughes, C.; Cassidy, E.; McClelland, K.; Odrzywol, E.; et al. Discovery and characterization of highly potent and selective allosteric USP7 inhibitors. *Nat. Chem. Biol.* **2018**, *14*, 118–125, doi:10.1038/nchembio.2528.
54. Lipinski, C.A.; Lombardo, F.; Dominy, B.W.; Feeney, P.J. Experimental and computational approaches to estimate solubility and permeability in drug discovery and development settings. *Adv. Drug Deliv. Rev.* **2001**, *46*, 3–26, doi:10.1016/s0169-409x(00)00129-0.
55. Hossain, M.U.; Khan, M.A.; Rakib-Uz-Zaman, S.M.; Ali, M.T.; Islam, M.S.; Keya, C.A.; Salimullah, M. Treating Diabetes Mellitus: Pharmacophore Based Designing of Potential Drugs from Gymnema

- sylvestre against Insulin Receptor Protein. *Biomed Res. Int.* **2016**, 3187647, doi:10.1155/2016/3187647.
56. Joseph, O.A.; Babatomiwa, K.; Niyi, A.; Olaposi, O.; Olumide, I. Molecular Docking and 3D Qsar Studies of C000000956 as a Potent Inhibitor of Bace-1. *Drug Res. (Stuttg)* **2019**, 69, 451–457, doi:10.1055/a-0849-9377.

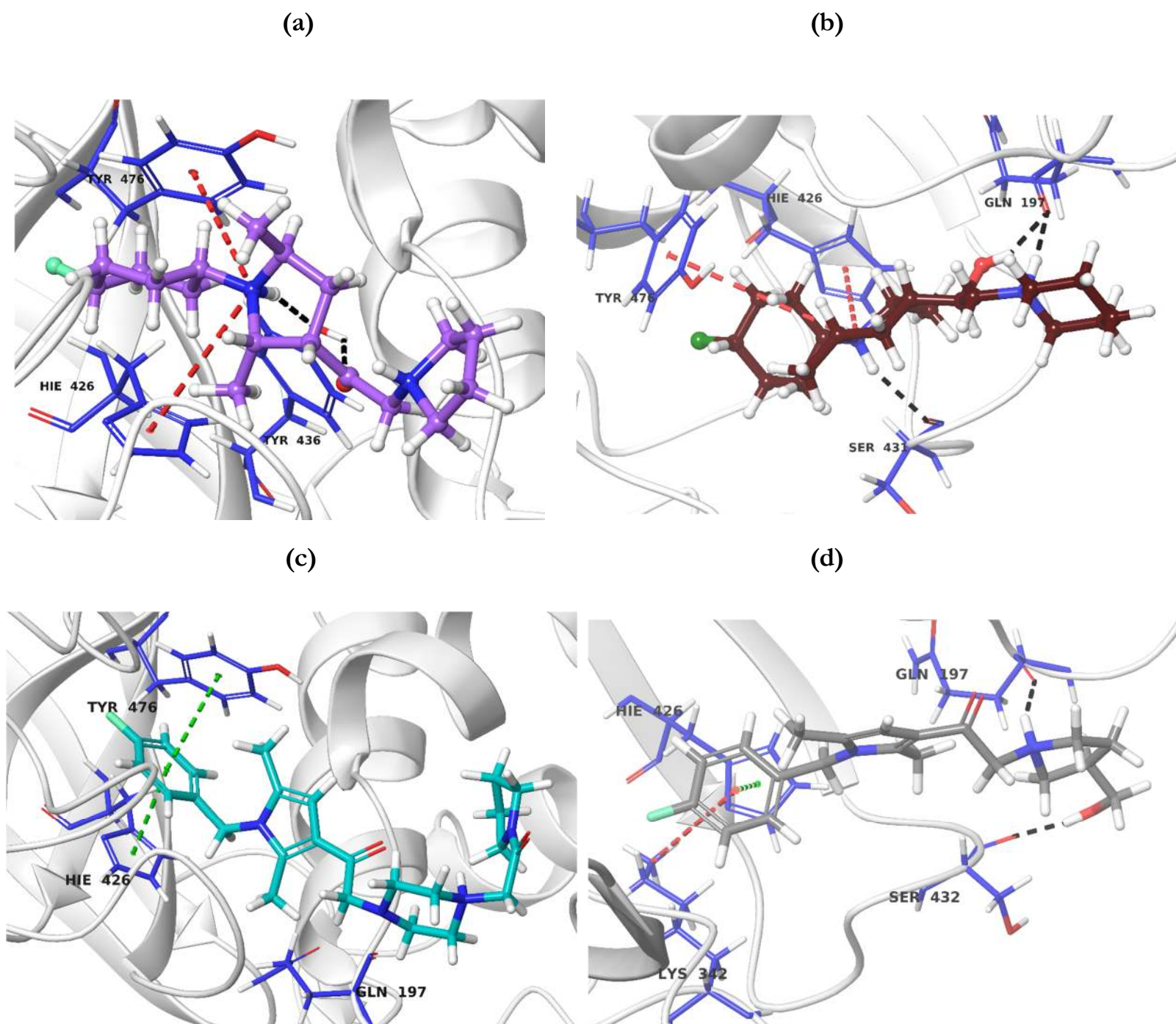


Figure 1. Interaction profile of the lead and reference compounds bound to USP14^{CAT} binding site after molecular docking studies in 3D. Interactions are shown in dotted lines; H-Bonds: blue, NH-- π : red, and π -- π : green interactions. **(a)** USP14^{CAT}-IU1 complex, **(b)** USP14^{CAT}-IU1-47 complex, **(c)** USP14^{CAT}-CID 43013232 complex, **(d)** USP14^{CAT}-CID 112370349 complex.

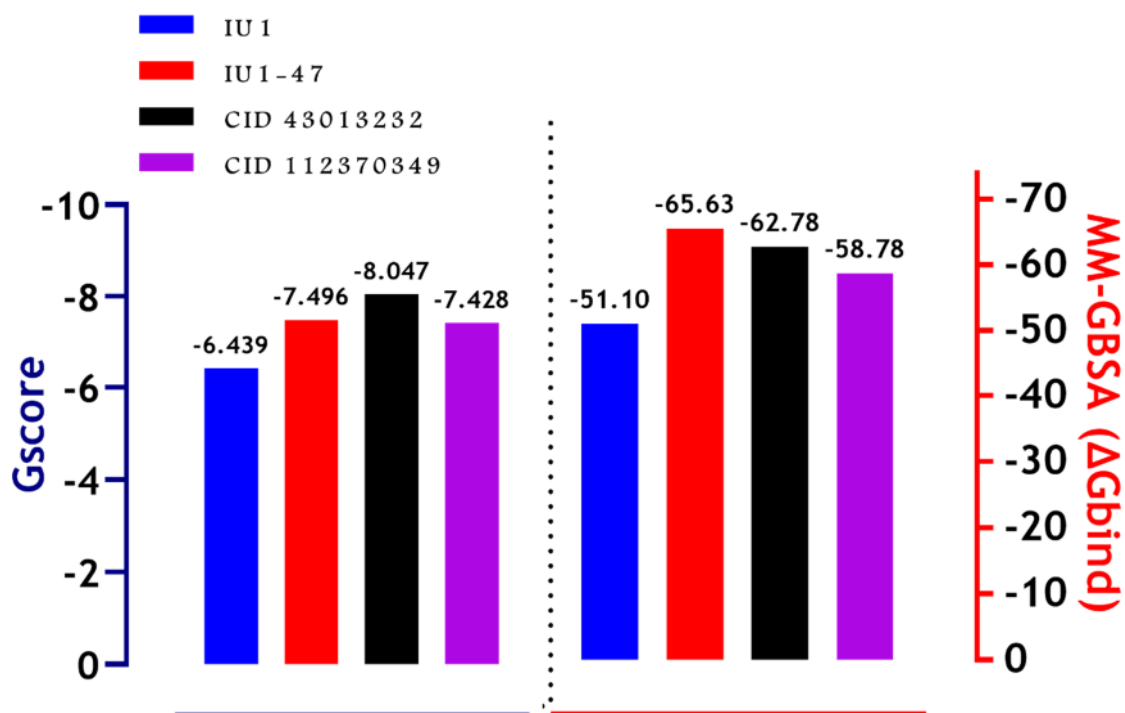


Figure 2. Molecular docking score (Gscore) and Prime/MM-GBSA binding energy (ΔG_{bind}) of the lead and reference compounds. The left frame (blue) shows the Gscore, while the right frame (red) displays the MM-GBSA binding energy.

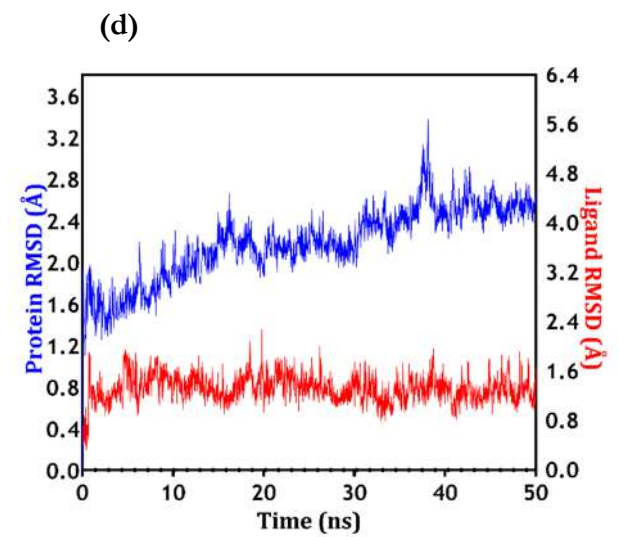
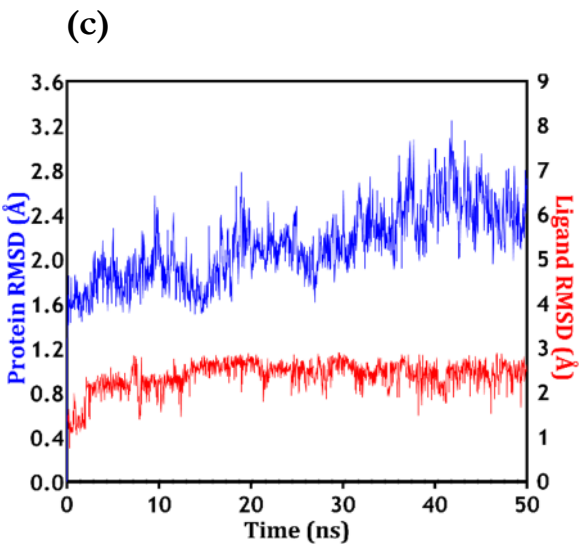
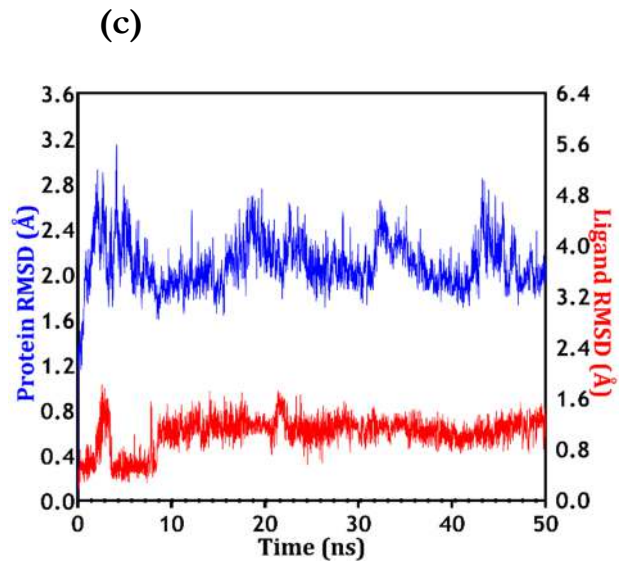
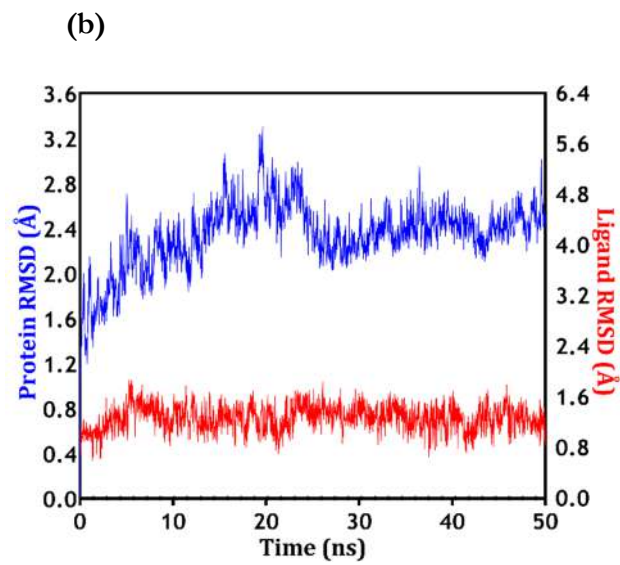
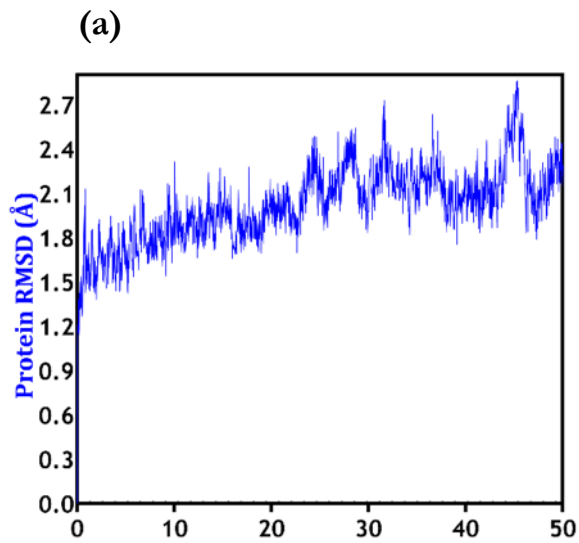


Figure 3. Line representation of the evolution of Root mean square deviation (RMSD) during the MD simulations of USP14^{CAT} complex with the lead and reference compounds. (a) APO USP14^{CAT}, (b) IU1, (c) IU1-47 (d) CID 43013232, and (e) CID 112370349. The left frame shows RMSD value for USP14^{CAT} C α , whereas the right frame shows the ligand RMSD value. Lig fit Lig shows the RMSD of the ligand that is aligned and measured on its reference (first) conformation.

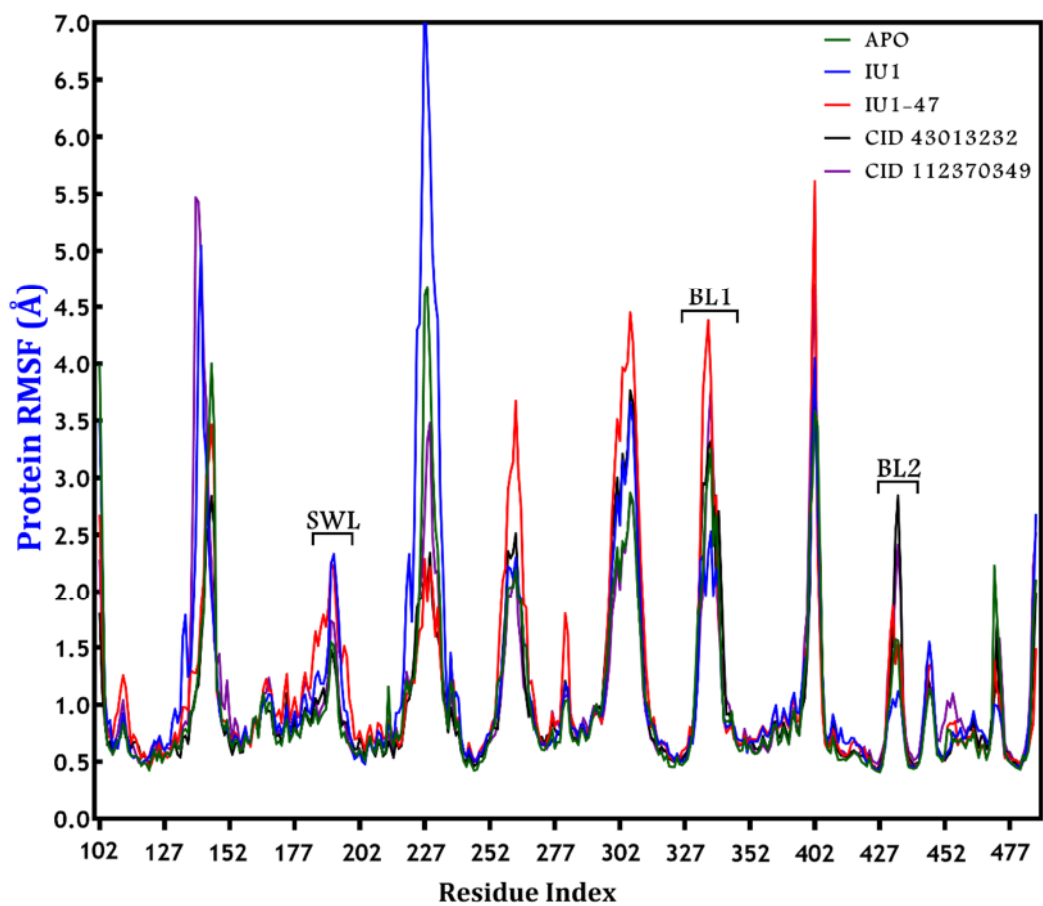


Figure 4. Line representation of the evolution of Root mean square fluctuation (RMSF) of USP14^{CAT} Cα during the MD simulations. Apo state: green, IU1: blue, IU1-47: red, CID CID 43013232: black, and CID 112370349: purple.



(a)

(b)

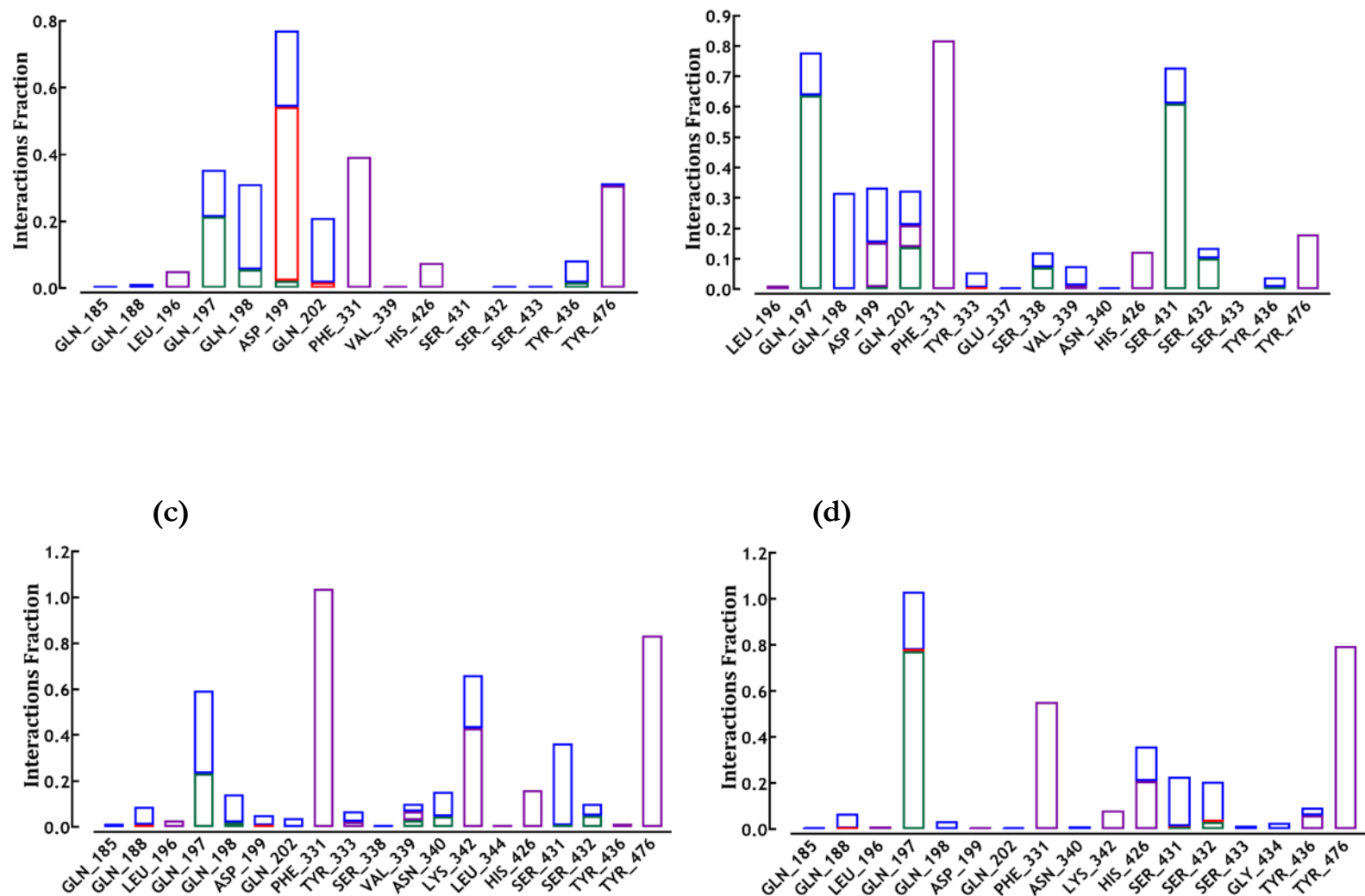


Figure 5. Percentage protein-ligands contacts monitored throughout 50ns simulation run time. The stacked bar charts show the different type of interactions between the ligands and the USP14; (a) USP14^{CAT}-IU1 complex, (b) USP14^{CAT}-IU1-47 complex, (c) USP14^{CAT}- CID 43013232 complex, (d) USP14^{CAT}- CID 112370349 complex. The legend above depicts the type of interactions that occurred by means of the colour code.

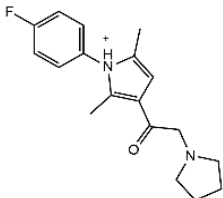
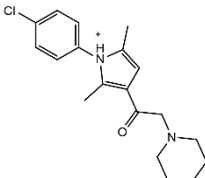
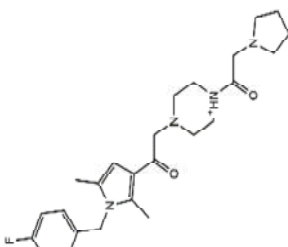
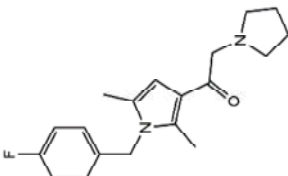
Table 1. Molecular recognition interactions between Lead and Standard molecules and USP14^{CAT} after molecular docking.

Compounds	H-Bond	NH---π/π---π Stacking Interactions	Hydrophobic Interactions
-----------	--------	---------------------------------------	--------------------------

IU1	Tyr436	Hie426, Tyr476	Phe331, Tyr436, Tyr476
IU1-47	Hie426, Tyr476	Hie426, Tyr476	Leu196, Phe331, Tyr436, Tyr476
CID 43013232		Hie426, Tyr476	Phe186, Leu196, Phe331, Tyr436, Tyr476
CID 112370349	Gln197, Ser432	Lys342, Hie426	Leu196, Phe331, Tyr436, Tyr476

Table 2. Drug-Likeness & ADME properties

Structure	mol MW	QPlogBB	QPPMDCK	#metab	QPlogKhsa	%HOA	ROF
-----------	--------	---------	---------	--------	-----------	------	-----

	IU1	300.375	0.587	1228.194	4	0.368	100	0
	IU1-47	330.856	0.609	9858.751	1	0.129	100	0
	43013232	440.56	0.362	146.242	7	-0.207	77.015	0
	112370349	3.44.428	-0.25	300.798	6	0.344	91.849	0

mol_MW, molecular weight: A.R.: 130–725; **QPlogBB**, predicted brain/blood partition coefficient, -3.0 to 1.2; **QPPMDCK**, predicted apparent Madin-Darby canine kidney cell permeability, <25 = poor, >500 = great; **QPlogKhsa**, prediction of binding to human serum albumin, -1.5 to 1.5; **HOA**, human oral absorption level, 1, 2, 3: 1 = low, 2 = medium; **ROF**, the number of violations of Lipinski's rule of five.

A.R., Accepted Range.